Carbon nanotube-polyoxometalate nanohybrids as efficient electro-catalysts for the hydrogen evolution reaction

Dhanaji Jawale, Frédéric Fossard, Frédéric Miserque, Valérie Geertsen, Anne-Lucie Teillout, Pedro de Oliveira, Israël Mbomekallé, Edmond Gravel, Eric Doris

Carbon nanotube-polyoxometalate nanohybrids as efficient electro-catalysts for the hydrogen evolution reaction

Dhanaji V. Jawale,[a,b,c] Frédéric Fossard,[d] Frédéric Miserque,[e] Valérie Geertsen,[f] Anne-Lucie Teillout,[b] Pedro de Oliveira,[b] Israël M. Mbomekallé,[*b] Edmond Gravel[*a] and Eric Doris[a]

a. Université Paris-Saclay, CEA, INRAE, Département Médicaments et Technologies pour la Santé (DMTS), SCBM, 91191 Gif-sur-Yvette, France.

b. Université Paris-Saclay, Institut de Chimie Physique, Equipe d'Electrochimie et de Photo-électrochimie, UMR 8000 CNRS, 91405 Orsay, France.

c. Department of Chemistry, Rishi Dayaram & Seth Hassaram National College and Seth Wassiamull Assomull Science College, Bandra (West), Mumbai 400 050, India.

d. Université Paris-Saclay, ONERA-CNRS, Laboratoire d'Etude des Microstructures, BP 72, 92322 Châtillon, France.

e. Université Paris-Saclay, CEA, DES-Service de la Corrosion et du Comportement des Matériaux dans leur Environnement (SCCME), 91191 Gif-sur-Yvette, France.

f. Université Paris-Saclay, CEA, CNRS, NIMBE, 91191 Gif-sur-Yvette, France.

Abstract

Electroactive hybrid nanomaterials were assembled by non-covalent, layer-by-layer deposition of tungsten-based polyoxometalates on carbon nanotubes. Chemical functionalisation permitted access to nanotubes densely and homogeneously covered with polyoxometalates. Electrochemical characterisation of the nanohybrids highlighted the beneficial contribution of the nanotube platform to the overall stability of POM, and to the enhancement of their catalytic performances when applied to the hydrogen evolution reaction.

Keywords

Carbon nanotube; functionalization; polyoxometalate; hydrogen evolution; electrocatalysis

[*] Corresponding authors: I. M. Mbomekalle, Tel: +33-169154159, E-mail: israel.mbomekalle@universite-paris-saclay.fr; E. Gravel, Tel: +33-169088484, E-mail: edmond.gravel@cea.fr

1. Introduction

In the context of renewable energies, hydrogen is regarded not only as a clean and sustainable carrier but also as the main alternative to carbon-based fuels.[1] Molecular hydrogen can be produced by electro-catalytic reduction of water (hydrogen evolution reaction - HER) but the current use of platinum in industrial electrolytic cells is a major drawback, due to the scarcity and cost of the precious metal. To make the HER technology economically viable and sustainable, platinum ought to be replaced by cost-effective and abundant materials.[2] In that regard, the molecular metal oxide clusters known as polyoxometalates (POMs) are promising candidates, as they can undergo reversible multivalent reduction/oxidation reactions, leading to the formation of mixed-valence species with favorable electro-catalytic properties.[3–6] Pioneering work on POMs applied to HER dates from 1985 with the seminal publication from Keita and Nadjo.[7] The electro-catalytic performances of POMs can be improved by immobilization on solid supports,[8] including nanostructured materials which offer high specific surface areas and tridimensional networks that are beneficial in terms of loading, stability and active site accessibility. Among these materials, carbon nanotubes (CNTs) combine the above advantages together with excellent electronic conductivity that is highly sought for the preparation of electrodes to be used in electro-catalytic devices.[9] However, POM immobilization by covalent functionalization of CNTs leads to some degradation of the nanotube surface that, in turn, alters their electronic properties. On the other hand, CNTs can be functionalized by non-covalent processes, without affecting the graphitic network. However, the latter functionalization processes classically provide unstable assemblies and limited density of decoration. Some of us have long been involved in the development of strategies for the immobilization of catalytic species on CNTs, *via* a layer-by-layer approach.[10–17] The method fully preserves the integrity of the carbonaceous support and allows for dense, homogeneous and stable anchoring of the active components at the surface of the nanotubes. With these features in mind and as part of our interest in CNT-based heterogeneous systems applied to electro-catalysis,[18–21] we report here the robust supramolecular assembly of POMs on CNTs and the evaluation of the resulting nanohybrids as electro-catalysts for the hydrogen evolution reaction.

2. Material and methods

2.1. Electrocatalyst preparation by assembly of POMs on CNT

2.1.1. Material

Chemicals were purchased from Sigma–Aldrich and used without further purification. Multi-walled carbon nanotubes were prepared by catalytic decomposition of methane on a Ni-MgO catalyst.[22]

Raw MWCNTs were purified by treatment with 8N HNO_3 for 12 h under refluxing conditions. DANTA was synthesised according to our previously reported procedure.[23]

2.1.2. Self-assembly and polymerization of DANTA amphiphile on CNT

DANTA (60 mg) was dissolved in 25 mM Tris aqueous buffer (6 mL, pH 8) before MWNTs (150 mg) were added. After 10 min of sonication with an ultra-sonic probe (5 min, 300 ms pulses per second, 25 W output power) a stable suspension was obtained and transferred into Eppendorf® tubes (6 × 1.5 mL) and centrifuged (5000 ×*g*, 3 min) to remove amorphous carbon. The supernatants were collected and centrifuged (15000 ×*g*, 45 min) to separate the DANTA-decorated nanotubes from amphiphile in excess. The supernatant was discarded while the pellets were resuspended in fresh Tris-buffer and centrifuged again (15000 ×*g*, 45 min). The final pellets were resuspended in buffer (4.5 mL) and submitted to UV irradiation (254 nm, 8 h) to polymerise the diacetylene groups and yield stabilised nanoring assemblies. Polymerization reinforces the cohesion of amphiphiles on the surface of the nanotube and leads to more robust assemblies.

2.1.3. Assembly of the second PDADMAC layer on the nanoring-coated nanotubes

After polymerization, the Tris-buffer volume was adjusted to 4.5 mL and the suspension was stirred in the presence of PDADMAC (2.1 mL of a 20% water solution) for 1 h to permit the formation of the two-layer assembly. Polymer in excess was removed by centrifugation (15000 ×*g*, 30 min) and the pellets were re-suspended in Tris-buffer (1.5 mL). This operation was repeated twice with Tris-buffer and two more times with pure water. The final pellets were combined and re-suspended in water (1 mL).

2.1.4. Deposition of POMs on CNTs

A representative procedure is given for the deposition of **{W_{18}}** on the coated CNTs: the multilayered nanotubes (200 µL of the above-described suspension) were transferred to an Eppendorf® tube before **{W_{18}}** (1 mL of a 10 mM solution/H_2O) was added. The mixture was left at room temperature with 1 min vortex-stirring every 30 min, for 4 h. The suspension was then centrifuged at 3000 ×*g* for 5 min and the nearly colorless supernatant was discarded and replaced with fresh aqueous solution of **{W_{18}}** (1 mL, 10 mM). The same process was repeated two more times to ensure optimal loading of the tubes with **{W_{18}}**. The final pellets were washed 3 times by centrifugation/redispersion in water. Finally,

water (200 µL) was added to yield the **{W_{18}}CNT** suspension that was used as such in electro-catalysis experiments.

2.2. Electrochemistry

2.2.1. Material

Pure water was obtained with a Milli-Q Intregral 5 purification set. High-purity grade H_2SO_4 was purchased from Sigma Aldrich and used without further purification. The composition of the medium was as follows: 0.5 M H_2SO_4 / pH 0.3. All POMs and their hybrid derivatives are sufficiently stable to be characterised in this medium. Electrochemical data were obtained using an EG & G 273 A potentiostat driven by a PC (M270 software). A divided cell with a standard three-electrode configuration was used for cyclic voltammetry experiments. The reference electrode was a saturated calomel electrode (SCE) and the counter electrode a glassy carbon plate of large surface area. The two electrodes were separated from the bulk electrolyte solution *via* fritted compartments filled with the same electrolyte. The working electrode was a 3 mm outer diameter glassy carbon (GC) from Mersen (France).

2.2.2. GC electrode pre-treatment

The electrode is polished for 5 min with a diamond paste of 6 µm grain size, then another 5 min with a diamond paste of 3 µm grain size, and finally immersed in pure water and subject to ultrasound sonication for 5 min. A volume of 3 µL of the suspension containing the material, previously homogenised by ultrasound sonication, is deposited on the surface of the GC electrode, which is left to dry in the open air overnight (at least for 12 h).

2.2.3. General experimental considerations

Before use, the modified electrode is immersed in the electrolyte for 5 min in order to release in the solution all traces of soluble or insoluble materials not solidly adsorbed on its surface. Prior to each experiment, solutions were thoroughly de-aerated for at least 30 min with pure argon. A positive pressure of this gas was maintained during subsequent work. The potentials are quoted against SCE unless otherwise stated and all experiments were performed at room temperature. Results were reproducible from one experiment to the other and the slight variations observed over successive runs are attributed to the uncertainty associated with the detection limit of our equipment (potentiostat, hardware and software) and not to the working electrode pre-treatment nor to possible fluctuations

in temperature. For comparison, CVs were recorded under the same conditions with solutions containing the free POMs used to obtain the hybrids (polyanion concentrations: 0.5 mM).

3. Results and discussion

3.1. Immobilization of POMs on CNTs

Polyoxometalates are anionic molecular metal oxides based on early, high-valent transition metals.[24] Four different tungsten-based POMs (Figure 1), namely Dawson-type $[P_2W_{18}O_{62}]^{6-}$ (**{W_{18}}**), $[P_2W_{17}Ni(OH_2)O_{61}]^{8-}$ (**{$W_{17}Ni$}**), and sandwich-type $[(P_2W_{15}O_{56})_2Ni_2(NaOH_2)_2]^{18-}$ (**{$W_{30}Ni_2$}**), $[(P_2W_{15}O_{56})_2Ni_2(NiOH_2)_2]^{16-}$ (**{$W_{30}Ni_4$}**) were synthesized[25–28] and immobilised at the surface of CNTs, following a layer-by-layer procedure that was adapted from our previous reports.[29,30]

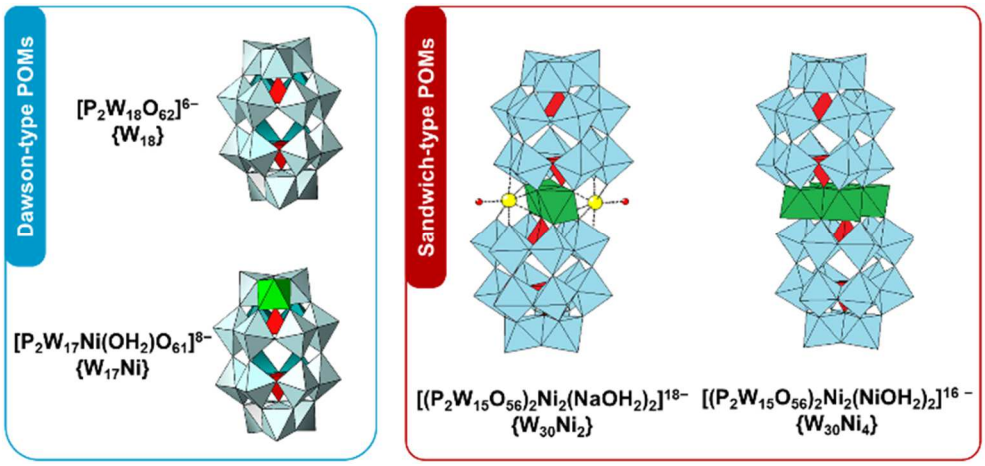

Figure 1. Structures of the different POM species.

Briefly, multi-walled carbon nanotubes were first sonicated in an aqueous suspension of diacetylene-nitrilotriacetate (DANTA) amphiphiles bearing a polar nitrilotriacetic head group and a diacetylene lipophilic chain. The choice of DANTA amphiphile as primary layer was governed by key benefits, including: i) the excellent dispersion of all kinds of CNTs (notwithstanding their surface oxidation state), ii) the formation of dense nanoring-like structures around the tubes that can be photopolymerized, iii) the stability of the polymerized nanorings which are resistant to dialysis and organic solvents washings, and iv) the creation of an array of anionic charges (NTA head groups) that are used to further functionalize the assemblies with a cationic polymer, interfacing with POMs. [29] Other surfactants and/or polymers have previously been investigated in our group but provided poorer assemblies in terms of stability and/or homogeneity of decoration.

Under ultrasound in aqueous suspension, DANTA self-organized at the surface of the CNTs into nanoring-like structures having their lipophilic chains in contact with the hydrophobic surface of the CNTs and their polar heads interfacing with water. Subsequent UV irradiation of the rings at 254 nm triggered the photopolymerization of neighboring diacetylene units. This 1,4-topochemical polymerization process led to the formation of a conjugated ene–yne network within the core of individual nanorings and reinforced the architecture of the assembly around the CNTs. The water-dispersible nanoconstructs (CNT-DANTA) display high density of anionic carboxylates on their surface, which allows for electrostatic deposition of a second cationic layer of poly(diallyldimethylammonium) chloride (PDADMAC). Finally, anionic POMs are added to the CNT-aqueous suspension. The tridimensional network of ammonium groups[31] acts as an anchoring and stabilizing environment for the negatively charged POMs that become tightly bonded to the CNT surface (Figure 2). After careful washing by several successive centrifugation/dispersion cycles, the four **{POM}CNT** hybrids were obtained as aqueous suspensions that were further characterised.

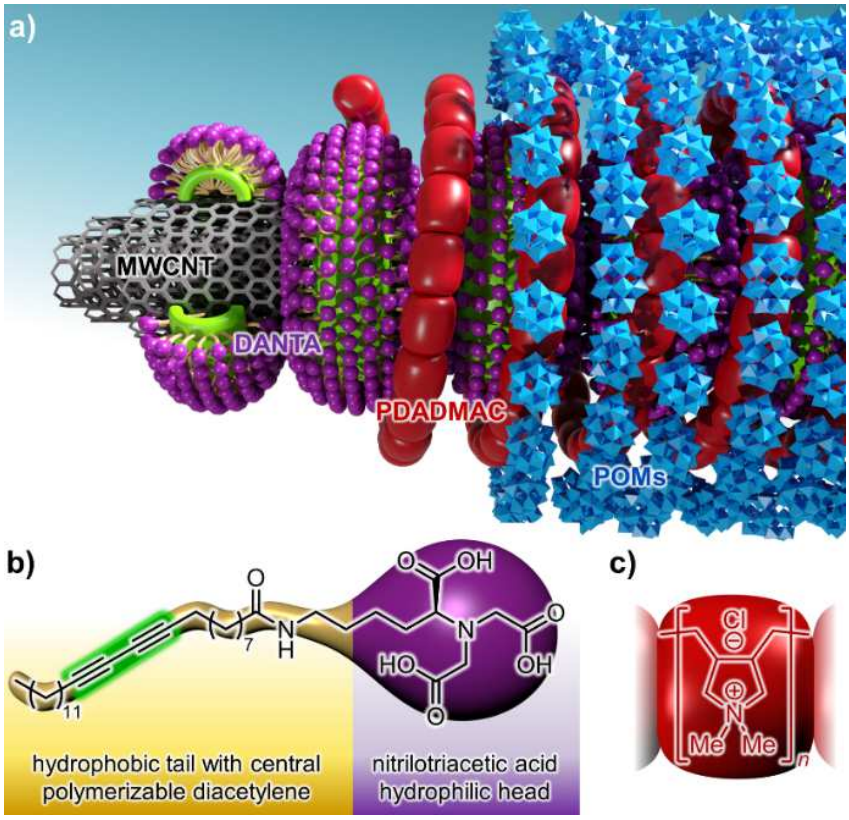

Figure 2. a) Overview of the {**POM}CNT** assembly; b) Structure of DANTA; c) Structure of PDADMAC.

3.2. Characterisation of the nanohybrids

Quantitative assessment of the tungsten content of the nanohybrid suspensions was obtained by inductively coupled plasma mass spectrometry (ICP-MS) analyses carried out on digested samples (by H_2O_2 treatment).[32] ICP-MS permitted the quantification of the POM concentration in the four nanohybrid aqueous suspensions (Table 1).

Table 1. POM and tungsten contents in the hybrid suspensions as determined by ICP-MS analysis.

	{W_{18}}CNT	**{$W_{17}Ni$}CNT**	**{$W_{30}Ni_2$}CNT**	**{$W_{30}Ni_4$}CNT**
{POM} (μM)	5.6	10.6	9.7	4.7
W (μM)	100	180	290	140

The morphology of the **{POM}CNT** assemblies was investigated by scanning transmission electron microscopy (STEM) using a high angle annular dark field (HAADF) detector carried out in parallel with energy-dispersive X-ray spectroscopy (EDS). The analysis performed on the different samples allowed the mapping of C, W, and Ni elements present in the constructs. Figure 3 shows **{$W_{30}Ni_2$}POMs** regularly and densely distributed at the surface of the CNTs, with co-localization of Ni and W (for other **{POM}CNT** assemblies mapping, see Figures S1-S3 in Appendix A).

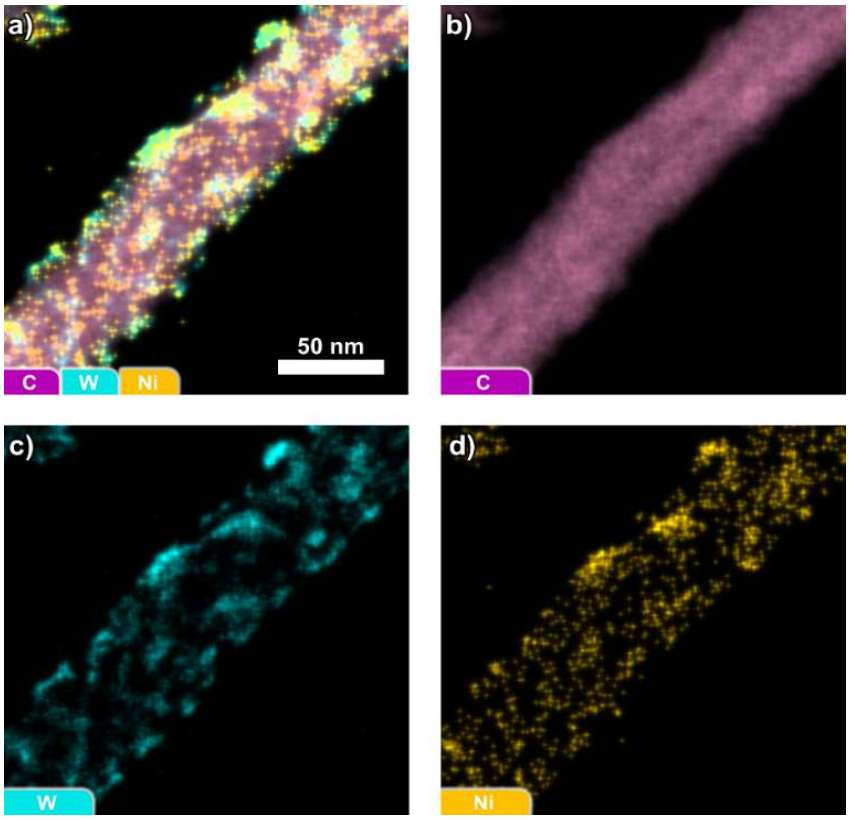

Figure 3. EDS mapping of the **{$W_{30}Ni_2$}CNT** assembly showing selected elements: a) merged; b) carbon; c) tungsten; d) nickel.

3.3. Electrochemical evaluation: POM *vs* {POM}CNT

3.3.1. {W_{18}} and {$W_{17}Ni$} in solution and on CNT

Cyclic voltammograms of freestanding **{W_{18}}** (in solution) and CNT-immobilised POMs (*i.e.* **{W_{18}}CNT**) deposited on a GC electrode, were recorded in 0.5 M H_2SO_4 (pH 0.3) at a scan rate of 100 mV s^{-1}. The two systems show roughly the same characteristics in terms of number of redox steps, peak potentials, the peak currents remaining proportional to the number of electrons exchanged in each step (Figures 4a/4b and Table S1 in Appendix A). These observations suggest that anchoring on CNTs did not alter the structure of POMs, although the first and second steps are, to some extent, merged for **{W_{18}}CNT**. The study of the peak current variation as a function of the square root of the scan rate (or the scan rate), indicated that, in solution, the electron transfer process is controlled by diffusion of **{W_{18}}**. It also validated that **{W_{18}}CNT** is successfully immobilised at the surface of the electrode (Figures S4 and S5). This is further supported by the sharp shape of the waves (Figure 4b) characteristic of species adsorbed on the working electrode surface and by the differences between the oxidation and reduction peak potentials, $\Delta E = E_a - E_c$, lower than those of the species in solution (Table S1).[33]

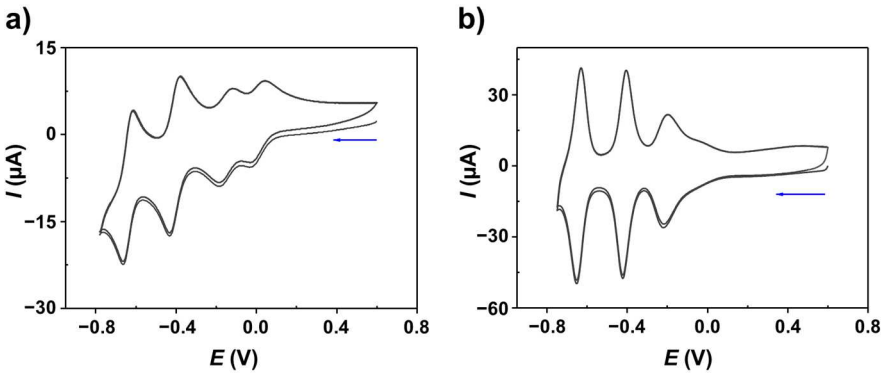

Figure 4. CVs of a) **{W_{18}}** in solution (0.5 mM); b) **{W_{18}}CNT** deposited on the working electrode. Electrolyte: 0.5 M H_2SO_4, pH = 0.3. Working electrode: GC; counter electrode: Pt; reference electrode: SCE. Scan rate: 100 mV s^{-1}.

In the case of **{W_{17}Ni}**, the reduction waves were attributed to the tungstic skeleton (Figure 5). Neither reduction nor oxidation of the Ni^{II} centre were detected in the range of potentials applied. However, upon successive cycling, CVs evolved as a function of both the applied potentials and the scan rates.

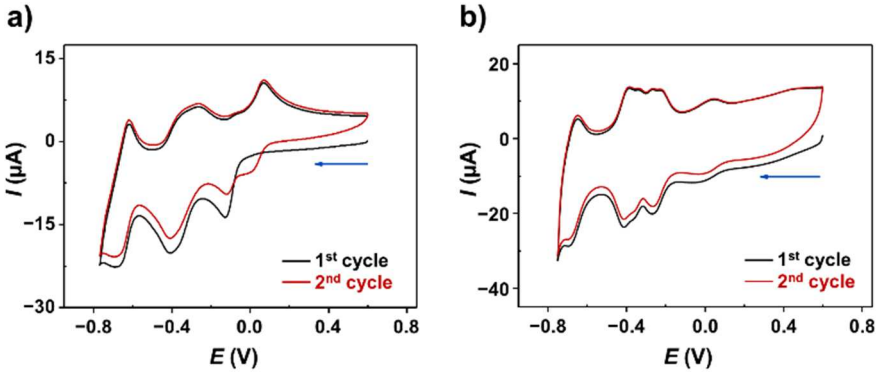

Figure 5. CVs of a) **{W_{17}Ni}** in solution (0.5 mM); b) **{W_{17}Ni}CNT** deposited on the working electrode. Electrolyte: 0.5 M H_2SO_4, pH = 0.3. Working electrode: GC; counter electrode: Pt; reference electrode: SCE. Scan rate: 100 mV s^{-1}.

Cycles were recorded between 0.6 V and −0.75 V *vs* SCE. In the first cycle **{W_{17}Ni}** exhibits three bi-electronic reduction waves located at −0.13 V, −0.41 V and −0.69 V *vs* SCE (black CV, Figure 5a). In the second scan, the first reduction wave splits into two single-electron reduction steps at 0.00 V and −0.12 V *vs* SCE (red CV, Figure 5a), but the following two reduction steps are not affected. If the potential is kept between 0.6 V and −0.25 V *vs* SCE, splitting is no longer observed, irrespective of the number of consecutive cycles (Figure S7c). Beyond this first wave, and when the scan includes the second reduction wave, E_r = −0.58 V *vs* SCE, the same phenomenon (splitting of the first reduction wave) is

again observed (Figures S7a and S7b). Another peculiarity is that re-oxidation is taking place in two single-electronic steps, during the backward scan. This phenomenon is prominent at low scan rates but tends to disappear at high scan rates (v > 100 mV s^{-1}) (Figure S8). The above observations can be rationalized by the following hypothesis: the reduced form of **{W_{17}Ni}** is not stable in solution and expels the Ni^{II} centre to give a **{W_{18}}**-like species. This is supported by the fact that the new reduction wave observed for **{W_{17}Ni}** is superimposable to the first wave of **{W_{18}}** (Figure S9). It is therefore important to find electro-catalytic conditions which favour the stability of the reduced form of **{W_{17}Ni}**, by preventing the release of nickel from the POM scaffold.

On the other hand, the CVs of **{W_{17}Ni}CNT** deposited on a GC electrode show no evolution over the consecutive cycles, whatever the range of the investigated potentials (Figure 5b). This suggests that **{W_{17}Ni}** deposited on CNTs is more robust and stable during reduction. There are four composite reduction waves (Table S1) that are all shifted towards positive potentials, compared to **{W_{17}Ni}** in solution (Figure S10a). **{W_{17}Ni}CNT** shows a better separated first reduction step and slightly more positive (E_c = 40 mV) than **{W_{18}}CNT**. The subsequent reduction waves are shifted to more negative potentials (Figure S10b, Table S1), and some splitting is observed. For example, the third reduction wave of **{W_{17}Ni}CNT** has two distinct peaks at −0.36 V and at −0.41 V *vs* SCE, and the backward scan also has two distinct re-oxidation steps at −0.34 V and at −0.39 V *vs* SCE. The second reduction wave has a single peak at −0.27 V *vs* SCE, while the associated re-oxidation wave has two distinct peaks at −0.23 V and −0.27 V *vs* SCE. These slight differences in the shape and position of the redox waves indicate that the immobilisation of **{W_{17}Ni}** on the CNTs has an impact on its redox behaviour, as anticipated. However, the CV retains its general shape, confirming that the structure and the electrochemical properties of the POM are preserved.

3.3.2. {$W_{30}Ni_2$} and {$W_{30}Ni_4$} in solution and on CNT

The redox behaviour of **{$W_{30}Ni_2$}** and **{$W_{30}Ni_4$}** in solution are very similar. There are four and three reduction waves, respectively, all attributed to the reduction of the tungstic skeleton (Table S2).[27] As opposed to **{W_{17}Ni}**, CVs of **{$W_{30}Ni_2$}** and **{$W_{30}Ni_4$}** in solution remain consistent during cycles, indicating greater stability of the reduced forms. The CV of **{$W_{30}Ni_2$}CNT** (on a GC electrode) resemble that of **{$W_{30}Ni_2$}** in solution. The number of redox waves is the same and the peak potential values are close (Figures 6a and 6b). There is, however, a more distinct separation between the first two redox steps of **{$W_{30}Ni_2$}CNT**, compared to **{$W_{30}Ni_2$}**.

To ensure that no POM is released in solution and demonstrate the stability of the assembly during the various characterisation cycles, a CV of the electrolyte that was used for several characterisation cycles was recorded on a bare polished glassy carbon electrode. Figure S11 shows superimposed CVs

of: i) the **{$W_{30}Ni_2$}CNT** species (red) and ii) a bare electrode in the previously used electrolyte (black). No trace of POM was detected in the latter by cyclic voltammetry. The absence of polyoxometalates in the electrolyte employed before was further confirmed by ICP-MS analyses.

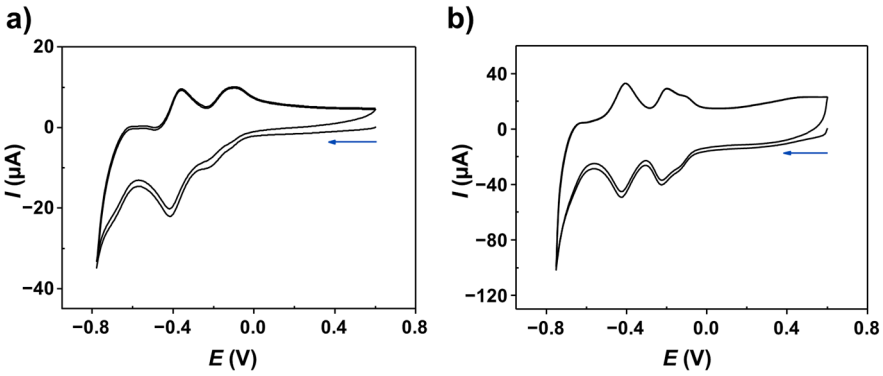

Figure 6. CVs of a) **{$W_{30}Ni_2$}** in solution (0.5 mM); b) **{$W_{30}Ni_2$}CNT** deposited on the working electrode. Electrolyte: 0.5 M H_2SO_4, pH = 0.3. Working electrode: GC; counter electrode: Pt; reference electrode: SCE. Scan rate: 100 mV s^{-1}.

For the POM containing four Ni^{II} centres, some marked changes in the CVs of **{$W_{30}Ni_4$}CNT** are observed with a new redox step resulting from the splitting of the first bi-electronic redox wave into two mono-electronic steps (Figures 7a and 7b, Table S2). Again, immobilization of **{$W_{30}Ni_4$}** on CNTs does not affect the overall redox properties (a comparative study of POMs directly deposited on the surface of GC electrodes is presented in Figure S12).

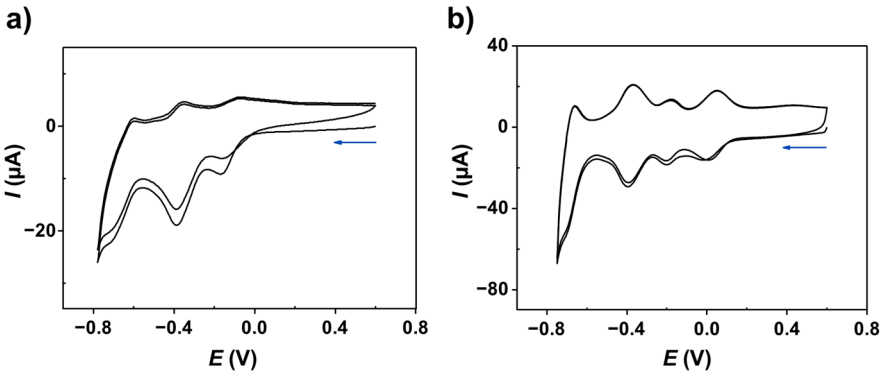

Figure 7. CVs of a) **{$W_{30}Ni_4$}** in solution (0.5 mM); b) **{$W_{30}Ni_4$}CNT** deposited on the working electrode. Electrolyte: 0.5 M H_2SO_4, pH = 0.3. Working electrode: GC; counter electrode: Pt; reference electrode: SCE; Scan rate: 100 mV s^{-1}.

3.3.3. Evaluation of the electro-catalytic properties using linear sweep voltammetry (LSV)

To complete their characterisation, the three nickel-containing materials were tested using LSV and a rotating disk electrode (RDE) after deposition on glassy carbon.

The study as a function of the potential scan rate confirms that the material is well deposited at the surface of the working electrode (Figures S13a and S13b). At low scan rates, $v < 20$ mV s^{-1}, it can be seen that, even for moderate overpotential values, $E > -0.75$ V *vs* SCE, the last reduction wave is already catalytic (red curves, Figure S14a). It is necessary to go beyond this threshold value to observe the same catalytic effect, the electro-reduction of protons, at higher scan rates (Figure S14b). As in the case of the cyclic voltammetry study, it can be concluded that two parameters have a decisive influence on the effectiveness of these modified electrodes as catalysts for the HER: i) the scan rate mentioned above and ii) the number of consecutive cycles plotted. The results of this study are thus in agreement with those obtained by cyclic voltammetry.

3.4. Hydrogen evolution reaction

To facilitate the evaluation of the catalytic efficiency and comparison of the nanohybrids, the measured currents are expressed hereafter as a function of the active surface area of the considered electrode. To observe an irreversible wave, characteristic of the electro-catalytic reduction of H^+, it was found necessary to go down to potential values close to −1.0 V *vs* SCE for POMs in solution. When the same POMs are deposited on CNTs, a gain in potential is observed, the value of which varies between 20 and 130 mV, and the current density is multiplied by a factor 2 to 8 (Figures S15, Table S3, Appendix A). The transitioning from POMs in solution to POMs deposited on CNTs thus improves the overall electro-catalytic performances of polyoxometalates.

In the case of POMs in solution, the surface of the GC working electrode does not undergo any noticeable change and is regenerated even when brought to low potential values (−1.0 V *vs* SCE, Figures S16). Gratifyingly, the behaviour of POM deposited on CNT is irreversible when the same potential values are applied to the electrode. In the case of **{W_{18}}CNT** electrode (no nickel), scanning of potentials to values as low as −1.0 V *vs* SCE leads to a drastic decrease in the peak currents of all the reversible redox waves observed between 0.60 V and −0.78 V *vs* SCE (Figure S17a). A similar phenomenon is observed with modified electrodes containing either **{$W_{17}Ni$}CNT** or **{$W_{30}Ni_2$}CNT**. The first two reversible redox waves disappear almost completely, while the last wave becomes fully irreversible (Figures S17b and S17c). Electrochemical activation of the electrode may therefore be assumed when brought to low potential values. The increase in the Ni^{II}/W^{VI} ratio accentuates this

phenomenon. In the case of the **{$W_{30}Ni_4$}CNT** electrode (four Ni^{II} centres), it is no longer necessary to reach values as negative as −1.0 V *vs* SCE to observe the same transformations. Several consecutive CVs recorded between 0.6 V and −0.78 V lead to the same observations (Figure S17d). In summary, except for **{$W_{30}Ni_4$}CNT**, if one does not go beyond the first reversible wave, *i.e.* −0.78 V *vs* SCE, the recorded CVs remain superimposable and no electro-catalytic reduction of protons is observed. Beyond this value, the modified electrodes are activated and HER is observed.

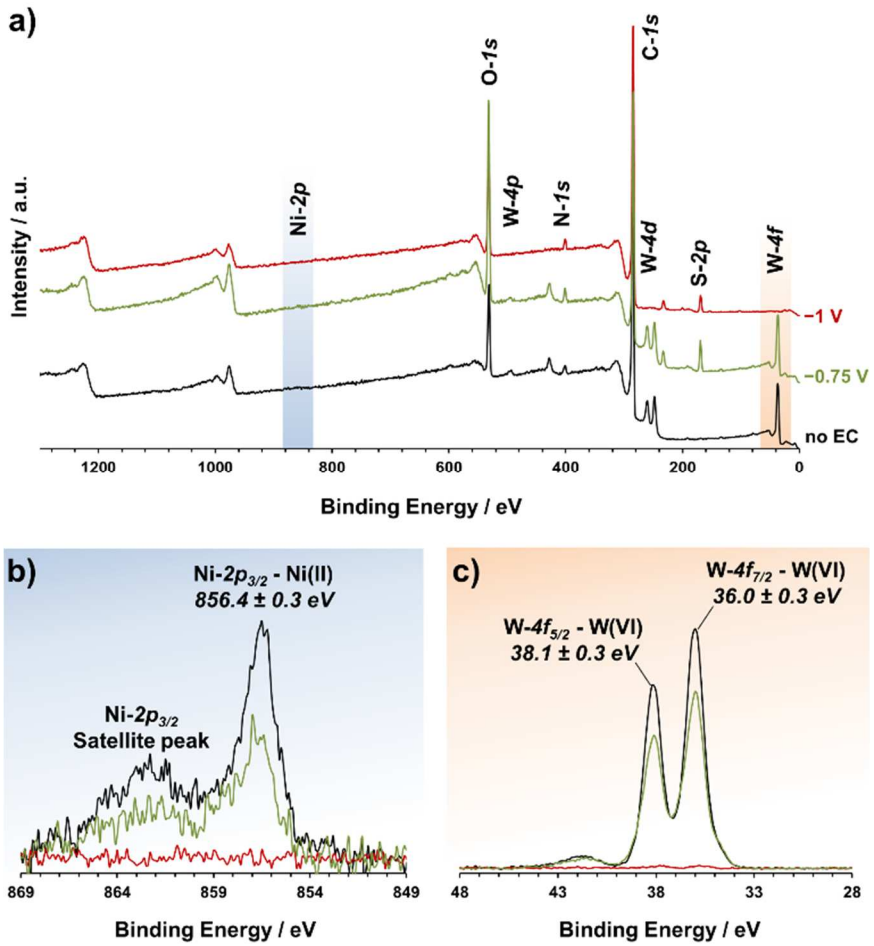

Figure 8. XPS analysis of the **{$W_{30}Ni_2$}CNT** hybrid before electro-catalysis (black line), after electro-catalysis at – 0.75 V (green line), and after electro-catalysis at – 1 V (red line). a) Global survey; b) Ni-*2p* region; c) W-*4f* region.

It thus appears that the most effective way to observe the electro-catalytic performances of the modified electrodes is to record CVs at low scan rates: 10 mV s^{-1} and 2 mV s^{-1} (Figure S18). Under these conditions, the HER takes place from −0.75 V *vs* SCE (for all four hybrid compounds) without electrode degradation. X-ray photoelectron spectroscopy (XPS) was performed on samples i) before electro-catalysis (Figure 8, black line), ii) after electro-catalysis at – 0.75 V (green line) and iii) after electro-

catalysis at –1 V (red line). These experiments show that the electrode surface composition remains the same if the limit value (E ≥ −0.75 V *vs* SCE) is not exceeded, which is in line with cyclic voltammetry results (Appendix C, Figure S26).

The scan rate selected to evaluate and compare catalytic efficiencies of the different electrodes is v = 2 mV s^{-1} (Figure S19). An important observation is the marked improvement in the electro-catalytic performances of each of the electrodes during successive cycles before stabilising. The electrodes remain stable and active for several months.

When comparing the CVs of the four nanohybrids deposited on CNTs, the POM/CNT without Ni^{II} centre (*i.e*. **{W_{18}}CNT**) gives the lowest current density and smallest potential gain (Figure S20). This observation suggests a beneficial contribution of Ni^{II}, as far as the HER is concerned. Although electrochemically silent, Ni^{II} centres embedded in the structure of POMs have a direct impact on the electro-catalytic properties, with respect to proton reduction (Table S5).[34]

Our primary objective was to improve the electro-catalytic properties of POMs by incorporating them in a nanostructured hybrid material through tailor-made assembly on CNT. The influence of the atomic percentage of nickel (ratio of the number of Ni centres to the total number of metal centres, *i.e.* Ni and W. %Ni = {[n(Ni) / [n(Ni) + n(W)]} × 100) was more particularly scrutinized and its influence on the overall catalytic performances tentatively rationalized. In the case of POMs in solution, our previous studies indicated that there is a direct correlation between Ni % and efficiency, with respect to HER (Table S5).[27,35] In order to achieve a relevant comparison of the performance of the different CNT-immobilised POMs, it is necessary to evaluate the electrochemically active surface area, Γ, and correct the current density values accordingly. In the case of an electroactive species adsorbed on the surface of a working electrode, the surface concentration of the species on the electrode is given by:

$$\Gamma = (4\, i_p\, R\, T) / (n^2\, F^2\, v\, A)$$

i_p = peak current

n = number of electrons transferred (4 in our case)

v = scan rate (0.1 V s^{-1})

A = geometric surface area of the electrode (0.0725 cm^2)

R = gas constant = 8.314 J mol^{-1} K^{-1}

T = room temperature = 298 K

F = Faraday constant = 96 485 C mol^{-1}

For this calculation we have taken into consideration the values of the reduction peak current intensities, i_{pc}, of the second tungsten reduction step (W_2) for a scan rate of v = 100 mV s^{-1}. The

corrected current densities, *J*, which take into account the electrochemically active surface area, are compiled in Table 2.

Table 2. Maximum electro-catalytic current as a function of the surface of the modified electrode, j_{max} (current density), and maximum current density as a function of the surface concentration, Γ, of the species deposited on the electrode, J_{max}. Values measured at E = −0.75 V *vs* SCE.

Hybrid	j_{max} (mA cm^{-2})	Γ (µmol cm^{-2})	J_{max} (A mol^{-1} cm^{-2})
{W_{18}}CNT	0.830	172.61	1.188
{$W_{17}Ni$}CNT	5.09	94.14	4.037
{$W_{30}Ni_2$}CNT	2.64	34.70	13.055
{$W_{30}Ni_4$}CNT	2.21	32.5	7.877

The obtained results are in line with the expected evolution of current densities as a function of the nickel percentage. As expected, the electrode modified with **{$W_{17}Ni$}CNT** is the least efficient of the three nickel-containing electrodes (Figure 9). On the other hand, the electrode modified with POM/CNT containing two Ni^{II} centres appears to be the most efficient. This observation corroborates previous results obtained with cobalt analogues used for water oxidation electro-catalysis.[36] In fact, compounds that have only two "d" metal centres in the equatorial metal cluster have two vacant positions that are likely to favour substrate adhesion. Their catalytic efficiency is greater than that of compounds of the same family whose equatorial metal cluster is "saturated" with four "d" metal centres.

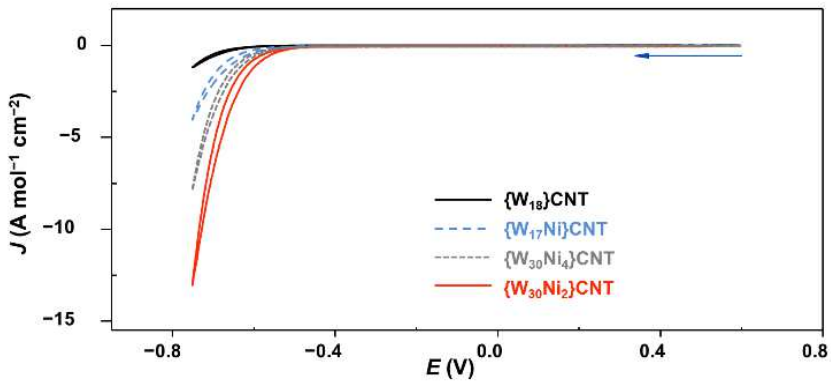

Figure 9. Comparison of the CVs obtained with POM/CNT hybrid materials deposited on a GC electrode. Current density, *J*, corrected with respect to the surface concentration of the hybrid deposited on the modified electrode. Electrolyte: 0.5 M H_2SO_4, pH = 0.3. Counter electrode: Pt; reference electrode: SCE. Scan rate: 2 mV s^{-1}.

Tafel plots were obtained (see Figure S21) based on the CVs of the four POM-CNT materials (Figure S20B). We found that calculated parameters (see Table S6) such as the slope values for POM-CNTs (comprised between −121 mV and −125 mV) are in the range of those of POM-based materials.[37] A direct comparison based on exchange current densities (j_0) values was carried out (see Table S7) and shows that the performances of our materials are also in line with previously reported systems.[38–46] However, it should be pointed out that this comparison is based on non-normalized values that do not take the catalyst surface concentration into consideration and thus may underestimate the activity of our best materials.

The catalytic efficiency of the three Ni-containing hybrids (investigated by LSV) follows the expected order, *i.e.* **{$W_{17}Ni$}CNT** < **{$W_{30}Ni_4$}CNT** < **{$W_{30}Ni_2$}CNT** (Figure S22a). This confirms the cyclic voltammetry results in the sense that the catalytic efficiency of these compounds towards the HER depends on both the number of Ni(II) centres and the structure of the POM. Quantification of this effect was attempted using RDE. However, the peculiarity of the HER, as seen on the LSVs, is that a current plateau is not reached and it is therefore difficult to apply the Levich equation model in this case. Nevertheless, the LSVs obtained by applying different electrode rotation rates, ranging between 100 and 3000 rpm, are presented in Figure S22b.

We did not observe any degradation in the catalytic performances of the POM-CNT over time, but rather a slight shift of the onset potential to less negative values. Figure S23 shows representative LSVs of the same **{$W_{30}Ni_2$}CNT**-modified electrode over a period of 9 days. Several hundred CVs and LSVs were recorded and, in addition to the shift of the onset potential, we also observed a more intense formation of H_2 bubbles at the surface of the electrode.

Finally, to benchmark our most active catalytic material (**{$W_{30}Ni_2$}CNT**), its performances were compared to those of platinum on charcoal. The CVs recorded at a scan rate of 100 mV s^{-1} show that the HER starts in the same potential range for the two electro-catalysts (Figure S24a). On the other hand, the LSVs (recorded with the same electrodes) at a scan rate of 2 mV s^{-1} indicate that the Pt-based material does outperform **{$W_{30}Ni_2$}CNT** to some extent in terms of the onset potential (corresponding to the start of the catalytic reaction) and catalytic current (Figure S24b). Yet, comparison with other POM-based materials (*e.g.* POM species deposited on Vulcan XC-72 carbon [38]) shows that **{$W_{30}Ni_2$}CNT** is more active as regards the onset potential values obtained under acidic conditions.

4. Conclusions

Nanohybrids were assembled from polyoxometalates on carbon nanotubes and used as efficient electro-catalysts for the production of hydrogen. Four different tungsten-based POM with varying numbers of nickel centres were studied. Electrochemical investigations highlighted that the CNT-based constructs exhibit improved stability and performances, compared to their unsupported counterparts. The hydrogen evolution reaction was also studied, with particular attention paid to the influence of the nickel centres in the POM structures. Our results highlight the benefits of heterogenisation in terms of catalytic activity. In fact, immobilised POMs show enhanced electro-catalytic properties compared to their free-standing counterparts, with lower onset potentials and higher current densities. The study also reveals that sandwich-type POM species with only two "d" metal centres in the equatorial metal cluster (and two vacant positions) are the most active catalysts, most likely because of favoured substrate adhesion.

Author contributions

D. V. Jawale: Investigation, Writing - Original Draft **F. Fossard:** Investigation **F. Miserque**: Investigation **V. Geertsen:** Investigation **A.-L. Teillout:** Conceptualization, Writing - Review & Editing **P. de Oliveira:** Conceptualization, Writing - Original Draft, Writing - Review & Editing **I. M. Mbomekallé:** Investigation, Conceptualization, Supervision, Writing - Original Draft, Writing - Review & Editing **E. Gravel:** Conceptualization, Supervision, Writing - Original Draft, Writing - Review & Editing **E. Doris:** Conceptualization, Supervision, Writing - Original Draft, Writing - Review & Editing

Acknowledgements

D. V. J. thanks the “Make our Planet Great Again” program and the “Initiative de Recherche Stratégique MOMENTOM” for support. Mrs. Elodie Barruet is gratefully acknowledged for technical assistance. The “Service de Chimie Bioorganique et de Marquage” (SCBM) belongs to the Laboratory of Excellence in Research on Medication and Innovative Therapeutics (ANR-10-LABX-0033-LERMIT) and is a partner of NOMATEN, a Centre of Excellence in Multifunctional Materials for Industrial and Medical Applications. The authors thank the CEA, the CNRS and the Université Paris-Saclay for financial support. HRSTEM-EDS study has benefited from the facilities of the Laboratory MSSMat (UMR CNRS 8579), CentraleSupélec.

References

[1] K. Mazloomi, C. Gomes, Hydrogen as an energy carrier: Prospects and challenges, Renew. Sustain. Energy Rev. 16 (2012) 3024–3033. https://doi.org/10.1016/j.rser.2012.02.028.

[2] G. Zhao, K. Rui, S.X. Dou, W. Sun, Heterostructures for Electrochemical Hydrogen Evolution Reaction: A Review, Adv. Funct. Mater. 28 (2018) 1803291. https://doi.org/10.1002/adfm.201803291.

[3] W. Liu, X.L. Wang, Y.Q. Lan, Polyoxometalates Assemblies and Their Electrochemical Applications, in: Song Y. F. (Ed.), Polyoxometalate-Based Assemblies and Functional Materials. Structure and Bonding, vol. 176, Springer Nature Switzerland AG, 2018, pp. 89–119. https://doi.org/10.1007/978-3-319-75904-3.

[4] C. Freire, D.M. Fernandes, M. Nunes, V.K. Abdelkader, POM & MOF-based Electrocatalysts for Energy-related Reactions, ChemCatChem 10 (2018) 1703–1730. https://doi.org/10.1002/cctc.201701926.

[5] N. Li, J. Liu, B.X. Dong, Y.Q. Lan, Polyoxometalate-Based Compounds for Photo- and Electrocatalytic Applications, Angew. Chem. Int. Ed. 59 (2020) 20779–20793. https://doi.org/10.1002/anie.202008054.

[6] M.R. Horn, A. Singh, S. Alomari, S. Goberna-Ferrón, R. Benages-Vilau, N. Chodankar et al., Polyoxometalates (POMs): from electroactive clusters to energy materials, Energy Environ. Sci. 14 (2021) 1652–1700. https://doi.org/10.1039/D0EE03407J.

[7] B. Keita, L. Nadjo, Activation of electrode surfaces: Application to the lectrocatalysis of the hydrogen evolution reaction, J. Electroanal. Chem. 191 (1985) 441–448. https://doi.org/10.1016/0022-0728(86)87056-5.

[8] A.S. Cherevan, S.P. Nandan, I. Roger, R. Liu, C. Streb, D. Eder, Polyoxometalates on Functional Substrates: Concepts, Synergies, and Future Perspectives, Adv. Sci. 7 (2020) 1903511. https://doi.org/10.1002/advs.201903511.

[9] Y. Ji, L. Huang, J. Hu, C. Streb, Y.-F. Song, Polyoxometalate-functionalized nanocarbon materials for energy conversion, energy storage and sensor systems, Energy Environ. Sci. 8 (2015) 776–789. https://doi.org/10.1039/C4EE03749A.

[10] D.V. Jawale, E. Gravel, E. Villemin, N. Shah, V. Geertsen, I.N.N. Namboothiri et al., Co-catalytic oxidative coupling of primary amines to imines using an organic nanotube–gold nanohybrid, Chem. Commun. 50 (2014) 15251–15245. https://doi.org/10.1039/C4CC07951E.

[11] D.V. Jawale, E. Gravel, C. Boudet, N. Shah, V. Geertsen, H. Li et al., Selective conversion of nitroarenes using a carbon nanotube–ruthenium nanohybrid, Chem. Commun. 51 (2015), 1739–1742. https://doi.org/10.1039/C4CC09192B.

[12] E. Gravel, I.N.N. Namboothiri, E. Doris, Supramolecular Assembly of Gold Nanoparticles on Carbon Nanotubes and Catalysis of Selected Organic Transformations, Synlett 27 (2016) 1179–1186. https://doi.org/10.1055/s-0035-15612881.

[13] P. Prakash, D. De Masi, V. Geertsen, F. Miserque, H. Li, I.N.N. Namboothiri et al., Selective Conversion of Nitroarenes to N-Aryl Hydroxylamines Catalysed by Carbon-Nanotube-Supported Nickel(II) Hydroxide, ChemistrySelect 2 (2017) 5891–5984. https://doi.org/10.1002/slct.201700876.

[14] P. Prakash, R. Arun Kumar, F. Miserque, V. Geertsen, E. Gravel, E. Doris, Carbon nanotube–copper ferrite-catalyzed aqueous 1,3-dipolar cycloaddition of in situ-generated organic azides with alkynes, Chem. Commun. 54 (2018) 3644–3647. https://doi.org/10.1039/C8CC00231B.

[15] G.A.M. Jardim, Í.A.O. Bozzi, W.X.C. Oliveira, C. Mesquita-Rodrigues, R.F.S. Menna-Barreto, R.A. Kumar et al., Copper complexes and carbon nanotube–copper ferrite-catalyzed benzenoid A-ring selenation of quinones: an efficient method for the synthesis of trypanocidal agents, New J. Chem. 43 (2019) 13751–13763. https://doi.org/10.1039/C9NJ02026H.

[16] E. Gopi, V. Geertsen, E. Gravel, E. Doris, Catalytic Dehydrosulfurization of Thioamides to Nitriles by Gold Nanoparticles Supported on Carbon Nanotubes, ChemCatChem 11 (2019) 5758–5761. https://doi.org/10.1002/cctc.201900377.

[17] E. Gopi, E. Gravel, E. Doris, Direct aerobic oxidation of alcohols into esters catalyzed by carbon nanotube–gold nanohybrids, Nanoscale Adv. 1 (2019) 1181–1185. https://doi.org/10.1039/C8NA00192H.

[18] N. Mackiewicz, G. Surendran, H. Remita, B. Keita, G. Zhang, L. Nadjo et al., Supramolecular Self-Assembly of Amphiphiles on Carbon Nanotubes: A Versatile Strategy for the Construction of CNT/Metal Nanohybrids, Application to Electrocatalysis, J. Am. Chem. Soc. 130 (2008) 8110–8111. https://doi.org/10.1021/ja8026373.

[19] A. Morozan, S. Donck, V. Artero, E. Gravel, E. Doris, Carbon nanotubes-gold nanohybrid as potent electrocatalyst for oxygen reduction in alkaline media, Nanoscale 7 (2015) 17274–17277. https://doi.org/10.1039/C5NR04576B.

[20] T.N. Huan, P. Prakash, P. Simon, G. Rousse, X. Xiangzhen, V. Artero et al., CO_2 Reduction to CO in Water: Carbon Nanotube–Gold Nanohybrid as a Selective and Efficient Electrocatalyst, ChemSusChem 9 (2016) 2317–2320. https://doi.org/10.1002/cssc.201600597.

[21] S. Donck, J. Fize, E. Gravel, E. Doris, V. Artero, Supramolecular assembly of cobaloxime on nanoring-coated carbon nanotubes: addressing the stability of the pyridine–cobalt linkage under hydrogen evolution turnover conditions, Chem. Commun. 52 (2016) 11783–11786. https://doi.org/10.1039/C6CC06059E.

[22] P. Chen, H.-B. Zhang, G.-D. Lin, Q. Hong, K.R. Tsai, Growth of carbon nanotubes by catalytic decomposition of CH_4 or CO on a Ni-MgO catalyst, Carbon 35 (1997) 1495–1501. https://doi.org/10.1016/S0008-6223(97)00100-0.

[23] D.V. Jawale, E. Gravel, C. Boudet, N. Shah, V. Geertsen, H. Li et al., Selective conversion of nitroarenes using a carbon nanotube–ruthenium nanohybrid, Chem. Commun. 51 (2015) 1739–1742. https://doi.org/10.1039/C4CC09192B.

[24] H.N. Miras, J. Yan, D.-L. Long, L. Cronin, Engineering polyoxometalates with emergent properties, Chem. Soc. Rev. 41 (2012) 7403–7430. https://doi.org/10.1039/C2CS35190K.

[25] I.M. Mbomekallé, Y.W. Lu, B. Keita, L. Nadjo, Simple, high yield and reagent-saving synthesis of pure α-$K_6P_2W_{18}O_{62}\cdot 14H_2O$, Inorg. Chem. Commun. 7 (2004) 86–90. https://doi.org/10.1016/j.inoche.2003.10.011.

[26] R. Contant, W.G. Klemperer, O. Yaghi, Potassium Octadecatungstodiphosphates(V) and Related Lacunary Compounds, Inorg. Synth. 27 (1990) 104–111. https://doi.org/10.1002/9780470132586.ch18.

[27] B.S. Bassil, A.M. Bossoh, M. Ibrahim, B. Avo Bile, A.S. Mougharbel, Z. Lin et al., Synthesis, Structure and Electrochemistry of the Dinickel(II)-Containing 30-Tungsto-4-Phosphate $[Ni_2Na_2(H_2O)_2(P_2W_{15}O_{56})_2]^{18-}$, Curr. Inorg. Chem. 7 (2017) 21–27. https://doi.org/10.2174/1877944107666171106162812.

[28] C.J. Comez-Garcia, J.J. Borras-Almenar, E. Coronado, L. Ouahab, Single-Crystal X-ray Structure and Magnetic Properties of the Polyoxotungstate Complexes $Na_{16}[M_4(H_2O)2(P_2W_{15}O_{56})_2]\cdot nH_2O$ (M = MnII, n = 53; M = NiII, n = 52): An Antiferromagnetic MnII Tetramer and a Ferromagnetic NiII Tetramer, Inorg. Chem. 33 (1994) 4016–4022. https://doi.org/10.1021/ic00096a028.

[29] J. John, E. Gravel, A. Hagège, H. Li, T. Gacoin, E. Doris, Catalytic Oxidation of Silanes by Carbon Nanotube–Gold Nanohybrids, Angew. Chem., Int. Ed. 50 (2011) 7533–7536. https://doi.org/10.1002/anie.201101993.

[30] D.V. Jawale, V. Geertsen, F. Miserque, P. Berthault, E. Gravel, E. Doris, Solvent-free hydrosilylation of alkenes and alkynes using recyclable platinum on carbon nanotubes, Green. Chem. 23 (2021) 815–820. https://doi.org/10.1039/D0GC03943H.

[31] D. Wang, S. Lua, S.P. Jiang, Pd/HPW-PDDA-MWCNTs as effective non-Pt electrocatalysts for oxygenreduction reaction of fuel cells, Chem. Commun. 46 (2010) 2058–2060. https://doi.org/10.1039/B927375A.

[32] P.C. Murau, Dissolution of Tungsten by Hydrogen Peroxide, Anal. Chem. 33 (1961) 1125–1126. https://doi.org/10.1021/ac60176a021.

[33] J.-M. Savéant, C. Costentin, Elements of Molecular and Biomolecular Electrochemistry: An Electrochemical Approach to Electron Transfer Chemistry, 2nd Edition, John Wiley & Sons Inc., 2019. https://doi.org/10.1002/9781119292364.

[34] D. Jabbour, B. Keita, I.M. Mbomekallé, L. Nadjo, U. Kortz, Investigation of Multi-Nickel-Substituted Tungstophosphates and Their Stability and Electrocatalytic Properties in Aqueous Media, Eur. J. Inorg. Chem. (2004) 2036–2044. https://doi.org/10.1002/ejic.200300830.

[35] B.S. Bassil, Y. Xiang, A. Haider, J. Hurtado, G. Novitchi, A.K. Powell et al., Heptanickel(ii) double-cubane core in wells-dawson heteropolytungstate, $[Ni_7(OH)_6(H_2O)_6(P_2W_{15}O_{56})_2]^{16-}$, Chem. Commun. 52 (2016) 2601–2604. https://doi.org/10.1039/C5CC09823H.

[36] C.S. Ayingone Mezui, P. de Oliveira, A.-L. Teillout, J. Marrot, P. Berthet, M. Lebrini et al., Synthesis, Structure, and Magnetic Electrochemical Properties of a Family of Tungstoarsenates Containing Just Co^{II} Centers or Both Co^{II} and Fe^{III} Centers, Inorg. Chem. 56 (2017) 1999–2012. https://doi.org/10.1021/acs.inorgchem.6b02593.

[37] C. Xu, J. Li, D. Sun, X. Li, X. Wang, Z. Su, Co/WC@NC electrocatalysts derived from polyoxometalates (POM) for efficient hydrogen evolution, Nanotechnology 32 (2021) 375602. https://doi.org/10.1088/1361-6528/ac084d.

[38] B. Keita, U. Kortz, L.R. Brudna Holzle, S. Brown, L. Nadjo, Efficient Hydrogen-Evolving Cathodes Based on Proton and Electron Reservoir Behaviors of the Phosphotungstate $[H_7P_8W_{48}O_{184}]^{33-}$ and the Co(II)-Containing Silicotungstates $[Co_6(H_2O)_{30}\{Co_9Cl_2(OH)_3(H_2O)_9(\beta\text{-}SiW_8O_{31})_3\}]^{5-}$ and $[\{Co_3(B\text{-}\beta\text{-}SiW_9O_{33}(OH))(B\text{-}\beta\text{-}SiW_8O_{29}OH)_2\}_2]^{22-}$, Langmuir 23 (2007) 9531–9534. https://doi.org/10.1021/la7016853.

[39] R.N. Biboum, B. Keita, S. Franger, C.P. Nanseu Njiki, G. Zhang, J. Zhang et al., Pd0@polyoxometalate nanostructures as green electrocatalysts: illustrative example of hydrogen production. Materials 3 (2010) 741–754. https://doi.org/10.3390/ma3010741.

[40] D. M. Fernandes, M. P. Araújo, A. Haider, A. S. Mougharbel, A. J. S. Fernandes, U. Kortz et al., Polyoxometalate-graphene Electrocatalysts for the Hydrogen Evolution Reaction, ChemElectroChem 5 (2018) 273–283. https://doi.org/10.1002/celc.201701210.

[41] B. Nohra, H. El Moll, L. M. Rodriguez Albelo, P. Mialane, J. Marrot, C. Mellot-Draznieks et al., Polyoxometalate-Based Metal Organic Frameworks (POMOFs): Structural Trends, Energetics, and High Electrocatalytic Efficiency for Hydrogen Evolution Reaction. J. Am. Chem. Soc. 133 (2011) 13363–13374. https://doi.org/10.1021/ja201165c.

[42] R.J. Liu, G.J. Zhang, H.B. Cao, S.J. Zhang, Y.B. Xie, A. Haider et al., Enhanced proton and electron reservoir abilities of polyoxometalate grafted on graphene for high-performance hydrogen evolution, Energy Environ. Sci. 9 (2016) 1012–1023. https://doi.org/10.1039/C5EE03503A.

[43] E.J. Popczun, C.G. Read, C.W. Roske, N.S. Lewis, R.E. Schaak, Highly Active Electrocatalysis of the Hydrogen Evolution Reaction by Cobalt Phosphide Nanoparticles, Angew. Chem., Int. Ed. 53 (2014) 5427–5430. https://doi.org/10.1002/anie.201402646.

[44] Y.-Y. Ma, C.-X. Wu, X.-J. Feng, H.-Q. Tan, L.-K. Yan, Y. Liu et al., Highly efficient hydrogen evolution from seawater by a low-cost and stable CoMoP@C electrocatalyst superior to Pt/C, Energy Environ. Sci. 10 (2017) 788–798. https://doi.org/10.1039/C6EE03768B.

[45] Q. Liu, J. Tian, W. Cui, P. Jiang, N. Cheng, A.M. Asiri et al., Carbon Nanotubes Decorated with CoP Nanocrystals: A Highly Active Non-Noble-Metal Nanohybrid Electrocatalyst for Hydrogen Evolution, Angew. Chem. Int. Ed. 53 (2014) 6710–6714. https://doi.org/10.1002/anie.201404161.

[46] D.M. Fernandes, M.P. Araújo, A.i Haider, A.S. Mougharbel, A.J.S. Fernandes, U. Kortz et al., Polyoxometalate-graphene Electrocatalysts for the Hydrogen Evolution Reaction, ChemElectroChem 5 (2018) 273–283. https://doi.org/10.1002/celc.201701210.